Nanoscale

Accepted Manuscript

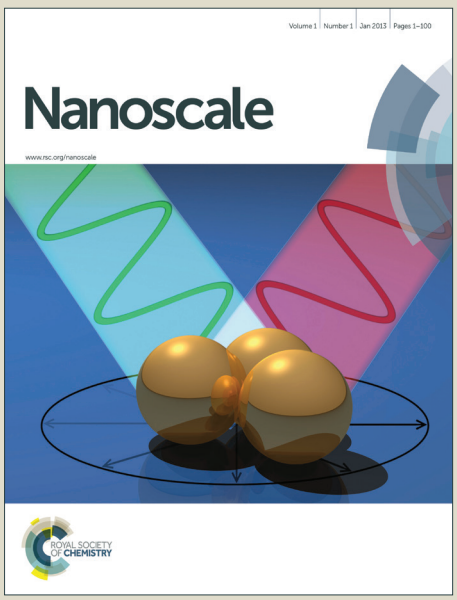

ROYAL SOCIETY OF CHEMISTRY

www.rsc.org/nanoscale

Graphical Abstract

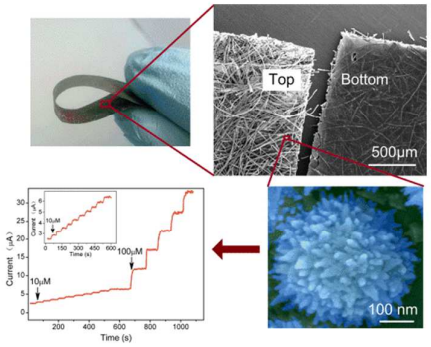

A free-standing graphene silk composite film decorated with spiky Pt nanospheres was prepared and utilized in electrochemical sensor applications.

Nanoscale

RSCPublishing

ARTICLE

Fabrication and application of flexible graphene silk composite film electrodes decorated with spiky Pt nanospheres

Cite this: DOI: 10.1039/xoxxoooooox

Received ooth January 2013,
Accepted ooth January 2013

DOI: 10.1039/xoxxoooooox

www.rsc.org/

Bo Liang, Lu Fang, Yichuan Hu, Guang Yang, Qin Zhu, and Xuesong Ye*

A free-standing graphene silk composite (G/S) film was fabricated via vacuum filtration of graphene oxide and silk fibres mixed suspension, followed by chemical reduction. Spiky structured Pt nanospheres were grown on the film substrate by cyclic voltammetry electrodeposition. Electrical and mechanical performances of a single graphene coated silk fibre were investigated. The conductivity of a single graphene coated silk fibre is 57.9 S m^{-1}. During 1000 times bending, the conductivities were stable and showed a negligible variation. The G/S film has a sheet resistivity of 90 Ω □$^{-1}$ with porous and hierarchical structure. The spiky Pt nanospheres decorated G/S film was directly used as a H_2O_2 electrode with a sensitivity of 0.56 mA mM^{-1} cm^{-2}, a linear range of 0 – 2.5 mM and a ultralow detection limit of 0.2 μM (S/N=3). A glucose biosensor electrode was further fabricated by enzyme immobilization. Results show a sensitivity of 150.8 μA mM^{-1} cm^{-2} and a low detection limit of 1 μM (S/N=3) for glucose detection. The strategy of coating graphene sheets on silk fibre surface provides a new approach for developing electrical conductive biomaterials, tissue engineering scaffolds, bendable electrodes, and wearable biomedical devices.

Introduction

Flexible electronics have aroused great interest in recent years because of their potential applications in modern and wearable electronics, compact energy devices, artificial skin, and advanced biomedical devices.[1-4] In biomedical field, flexible electrodes and biosensors are adhere to patients' bodies for health monitoring or implanted subcutaneous for long-term bio-signal measuring.[5] Flexible electrodes and biosensors can provide both mechanical modulus and shape matching to biological tissues due to their soft mechanical property and curvilinear layouts. To date, there are many materials have been developed for flexible electronics in industrial and biomedical applications. A conventional approach is depositing metal thin film on a flexible substrate, such as polyimide and polydimethylsiloxane.[6, 7] This method has been widely used in flexible printed circuit board industries. However, thin metal patterns can tolerate only limited deformation before breaking and peel off in harsh liquid chemical environment, which limits their applications in biomedical field. Paper-like graphene film is another flexible electrode material widely researched in recent years,[8-12] especially for energy storage applications.[13-18] Graphene film has several advantages, such as light weight, excellent mechanical strength, superior electrical conductivity, and chemical inertness.[19] However, graphene sheets tend to restack together due to van der Waals interactions[20-22] during the fabrication of graphene films and as a consequence form a densely packed layered structure. The densely packed layered structure lose many of the unique properties that individual graphene sheets possess, such as large specific surface area, high charge carrier mobility, excellent thermal conductivity and mechanical robustness.[23-25] Conductive textiles are another flexible materials used for ambulatory monitoring of bio-signals.[26, 27] Conductive textiles can be made with pure metal threads such as silver and stainless steel fibres,[27] or produced with insulated fibres including cotton, polyester, and nylon, coated with electrically conductive elements, like carbon, aluminium, copper, gold, or silver.[28-32] Electronic conductive coating of fibres leads to the development of smart clothing in daily life with electrodes, sensors, and circuits directly embedded in the clothes.

Silk has been a widely used textile since it was first developed in ancient China and distributed around the world via the Silk Road. Silk fibres are composed of fibrous proteins, known as fibroin, and sericin that surrounds the fibroin fibres and cements those together.[33] Natural silk fibres are electrical insulated. Coating silk fibres with electrically conductive elements makes the fibre conduct electricity. Polyaniline, a conductive polymer, is one of the coating materials.[34] However, the electrical conductivity of polyaniline depends on the type of dopant and degree of doping, and influenced by environment like solution pH. Evaporating gold on and around silk fibres can obtain flexible conductive microwires.[35, 36] However, gold sheath coated around the silk fibre decrease the elasticity of the fibre, and the gold coating layer is easy to crack during stretch and lost its conductivity. Recent research shows graphene oxide can combine with silk fibroin via hydrogen bonding, polar-polar, and hydrophobic-hydrophobic interactions and form high-strength structural materials.[37, 38] These results inspired us to directly coating graphene on silk fibres. Graphene is a light

material with an atom thick two-dimensional structure, excellent mechanical and electrical properties, and great flexibility. It will be a good choice for electrically conductive coating around fibres.

In this paper, we directly coated GO sheets on silk fibres by dyeing the fibres in GO suspension. After chemical reduction, GO sheets on the fibre surface were converted into graphene, which made the insulating silk fibres to be electrical conductive. Electrical and mechanical performances of a single graphene coated silk fibre were investigated. Electrical conductivity and mechanical robust property of the graphene coated silk fibre promise its applications for flexible biosensors and electronics. Graphene silk composite (G/S) film was then prepared by vacuum filtration of graphene oxide and silk fibres mixed suspension, followed by chemical reduction. The G/S film contains two sides with different morphology, one side porous and the other side compact. This unique structure makes the G/S film suitable for immobilization of electrochemical active nanoparticles and biomolecules. What's more, superior electrical conductivity of the G/S film allows it to be directly used as electrochemical electrode without needs of any additional binders or conductive substrates, which leads to a simplified and lightweight architecture. To demonstrate biosensor applications of the G/S film, a H_2O_2 electrochemical sensor was firstly prepared by electrodepositing Pt nanospheres on the G/S film. Surprisingly, Pt nanospheres grown on graphene coated silk fibres exhibit spiky nanostructures. The Pt nanosphere decorated G/S film shows superior catalytic performance in H_2O_2 oxidation. A glucose biosensor was then prepared by immobilizing glucose oxidases (GOx) on a Pt nanosphere decorated G/S film. The resulted biosensor shows high sensitivity, low detection limits, and good selectivity for glucose detection.

Experimental

Chemicals

Graphene oxide (GO) was obtained from Nanjing XFNANO Materials Tech Co., Ltd. (Nanjing, China). Silk fibres were prepared from B. mori silkworm cocoons purchased from a Chinese crude drug market. Glucose oxidase (GOx) from Aspergillus niger, chloroplatinic acid hexahydrate (H_2PtCl_6•$6H_2O$), and ascorbic acid were purchased from Aladdin Ltd. (Shanghai, China). All other reagents were purchased from Sinopharm Chemical Reagent Co., Ltd. (Shanghai, China) and were reagent grade. Deionized-ultrafiltered (18 MΩ•cm) water was used for all aqueous solutions.

Preparation of graphene coated silk fibres

Cocoons of B. mori silkworm were boiled for 60 min in an aqueous solution of Na_2CO_3 (0.05 M) and rinsed thoroughly with water to remove the glue-like sericin proteins. After dried at 65 ℃, silk fibres were immersed in 1 mg mL^{-1} GO suspension until thoroughly wet. Then the GO dyed silk fibres were collected and dried at 65 ℃. The dried GO coated silk fibres were immersed into an aqueous ascorbic acid solution (10 mg mL^{-1}) in boiling water bath and reacted about 1 h for reduction. After that the graphene coated silk fibres were collected, rinsed with water and dried at 65 ℃.

Preparation of G/S composite film

First, cocoons of B. mori silkworm were cut into small pieces with side length about 2 mm. Then, those small pieces of cocoons were boiled for 60 min in an aqueous solution of Na_2CO_3 (0.05 M) and infiltrated under evacuation followed by rinsing thoroughly with water to remove the glue-like sericin proteins. Last, Silk fibres were collected and dried at 65 ℃. Graphene silk composite (G/S) film was prepared as follows. First, graphene oxide silk composite (GO/S) film was prepared by infiltration of a GO and silk fibre composite suspension. Typically, 10 mg GO was dispersed in 20 mL deionized water with the aid of ultrasonic. After that, 50 mg silk fibres were added and dispersed by ultrasonic with mechanical stirring for 15 min to form a homogeneous composite suspension of GO and silk fibres. Then, the composite suspension was moved to a filter (5 cm in diameter, 0.22 μm pore size) and infiltrated under evacuation. A GO/S composite film was obtained by drying at 65 ℃ for 2 h and peeling off from the filter. The GO/S film containing filter was directly immersed into aqueous ascorbic acid solution (10 mg mL^{-1}) in boiling water bath and

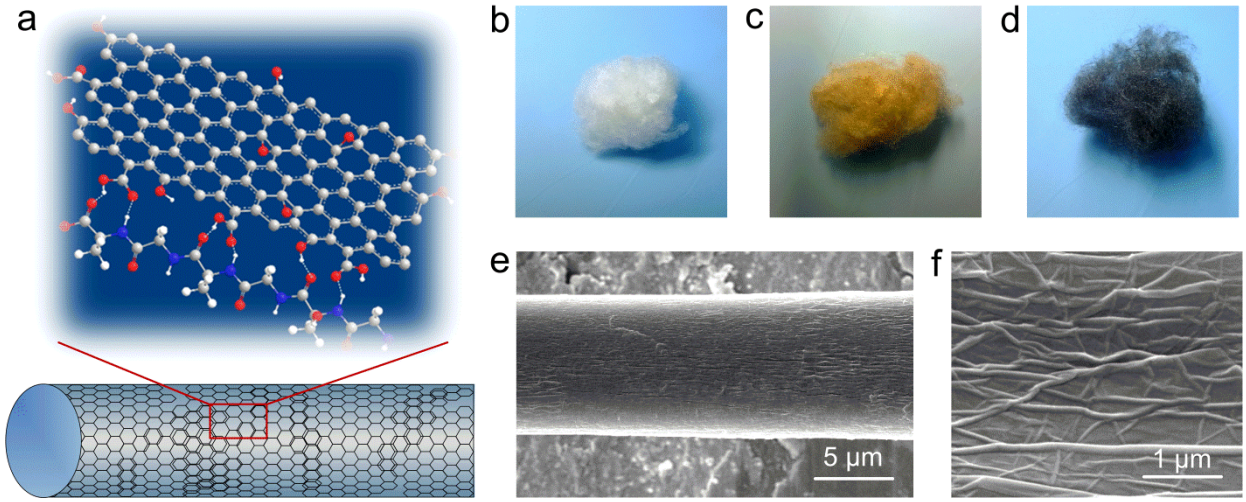

Fig.1 (a) Molecular model illustration of silk fibroin hydrophilic segments and graphene with polar interactions. (b-d) Digital photographs of pure silk fibres after removing of sericin (b), GO coated silk fibres (c), and graphene coated silk fibres (d). (e, f) SEM images of a graphene coated silk fibre.

reacted about 2 h for reduction. The colour of the film turned to black after the reduction. At last, the G/S film was then collected, washed with water 5 times, dried at 65 ℃, and peeled off from the filter. Various G/S films with different amount of GO and silk fibres were prepared for comparison. The G/S film was cut into required sizes for various tests using scissors.

Preparation of Pt nanosphere decorated electrodes

A piece of G/S film (5 mm by 5 mm) was clipped by a Pt electrode clamp and directly used as an electrochemical electrode. The deposition of Pt nanosphere was performed by CV scanning in the potential range from 0 to -0.6 V in a 10 mM H_2PtCl_6/0.1 M HCl solution at a scan rate of 50 mV s^{-1}. The Pt nanosphere decorated G/S film was directly used as a H_2O_2 detection electrode.

For preparation of a glucose sensor, a Pt nanosphere decorated G/S film was immersed in a glucose oxidase (GOx) solution comprising 10 mg mL^{-1} GOx and 30 mg mL^{-1} bovine serum albumin (BSA) in 0.01 M PBS (pH 7.4). After the G/S film was wet thoroughly, it was taken out and dried at room temperature. The enzyme coated G/S film was then exposed to a glutaraldehyde vapour in a sealed vial containing 50 μL glutaraldehyde (25%). The vial was kept at 35 ℃ for 3 h. The GOx was immobilized by cross-linking to the BSA. After that, the GOx immobilized G/S film was rinsed with water and dried at room temperature and the glucose biosensor was obtained.

Characterization

Scanning electron microscope (SEM) images were obtained using a thermal field emission scanning electron microscope (FSEM, SIRION-100, FEI, Netherlands), equipped to perform elemental analysis by energy dispersive X-ray spectroscopy (EDAX, USA). Raman spectra were acquired with a Jobin Yvon Raman spectrometer (LabRAM HR UV/Vis/NIR) using 514 nm laser excitation. Atomic force microscopy (AFM) was done using a scanning probe microscope (Pico scan 2100, Molecular Imaging Co.). X-ray photoelectron spectroscopy (XPS) analyses were carried out on an ESCALAB MARK II X-ray photoelectron spectrometer (VG Scientific Ltd., UK). Tensile tests were conducted with a dynamic mechanical analyser (DMA Q800, TA Instruments) in controlled strain rate mode with a strain ramp rate of 0.05% min^{-1}. Cyclic voltammetry, galvanostatic charge-discharge, electrochemical impedance spectroscopy, electrodeposition, and amperometric experiments were performed with a μAutolab III electrochemical workstation (Metrohm, Switzerland).

Results and discussion

Characterization of graphene coated silk fibre

Silk fibres produced by B. mori silkworm are composed of fibrous proteins, known as fibroin, and sericin that surrounds the fibroin fibres. Silk fibres after removing the glue-like sericin proteins are white in colour and show a natural shine (Fig. 1b). After GO coating, the fibres became deep yellow (Fig. 1c), suggesting GO was successfully absorbed on the surface of the fibres. The GO sheets deposited on a mica substrate (Fig. S1) are measured as thick as 0.8~1.2 nm, with an average lateral width of 1.0 μm, demonstrating the complete exfoliation in water. Chemical reduction of GO turned the fibres' colour from yellow to black (Fig. 1d). The resulting graphene coated silk fibres are robust, and no exfoliation of graphene sheets has been observed during bending process, suggesting that graphene sheets firmly attached to silk fibres via hydrogen bonding, polar-polar, and hydrophobic-hydrophobic interactions[37, 38] as illustrated in Fig. 1a. The morphologies of graphene coated silk fibres are further demonstrated by SEM. As shown in Fig. 1e and f, a wrinkled film was covered on the fibre surface, while the surface of pure silk fibre was very smooth without pleats (Fig. S2b).

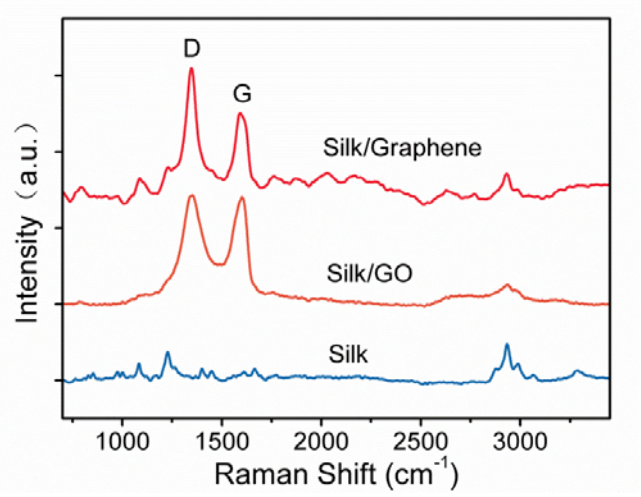

Fig. 2 Raman spectra of the pure silk fibre GO coated silk fibre, and graphene coated silk fibre.

Raman spectroscopy provides a powerful tool to study the surface compositions and microstructure of carbon-based materials. As shown in Fig. 2, the Raman spectrum of GO coated silk fibre displays two prominent peaks at 1353 and 1603 cm^{-1}, corresponding to the D and G bands, respectively. The G band is characteristic for sp^2-hybridized C-C bonds in a two-dimensional hexagonal lattice, while the D band corresponds to the defects and disorder in the planar carbon network,[39, 40] demonstrating that the silk fibre was covered with GO sheets. After the chemical reduction of GO, the D and G bands remain at the same position. However, the intensity ratio of D/G is increased obviously in comparison with that of the GO coated silk fibre spectrum, indicating the realization of deoxygenation and partially structure restoration in chemically reduced GO.[41-44] What's more peaks at 1084 cm^{-1}, 1227cm^{-1} and 2933 cm^{-1} attributed to the silk fibroin[45, 46] were observed obviously in the Raman spectrum of graphene coated silk fibre. However, these peeks are inconspicuous in the Raman spectrum of GO coated silk fibre. The reason might be that silk fibres were completely wrapped with GO sheets by the coating process (Fig. S3 a), after chemical reduction, GO sheets were reduced to graphene, and some sheets not attached firmly were flake off and some areas of silk fibres were exposed (Fig. S3 b).

The deoxygenation and partially structure restoration of GO was also confirmed by XPS spectra of GO before and after chemical reduction (Fig. S4). As shown in the full range XPS spectra (Fig. S4 a, b), the increased C/O ratio suggests that most of oxygen-containing groups are removed during the chemical reduction. The C1s high-resolution XPS spectra further revealed that most of the epoxy and hydroxyl groups of GO were successfully removed after the reaction (Fig. S4 c, d).

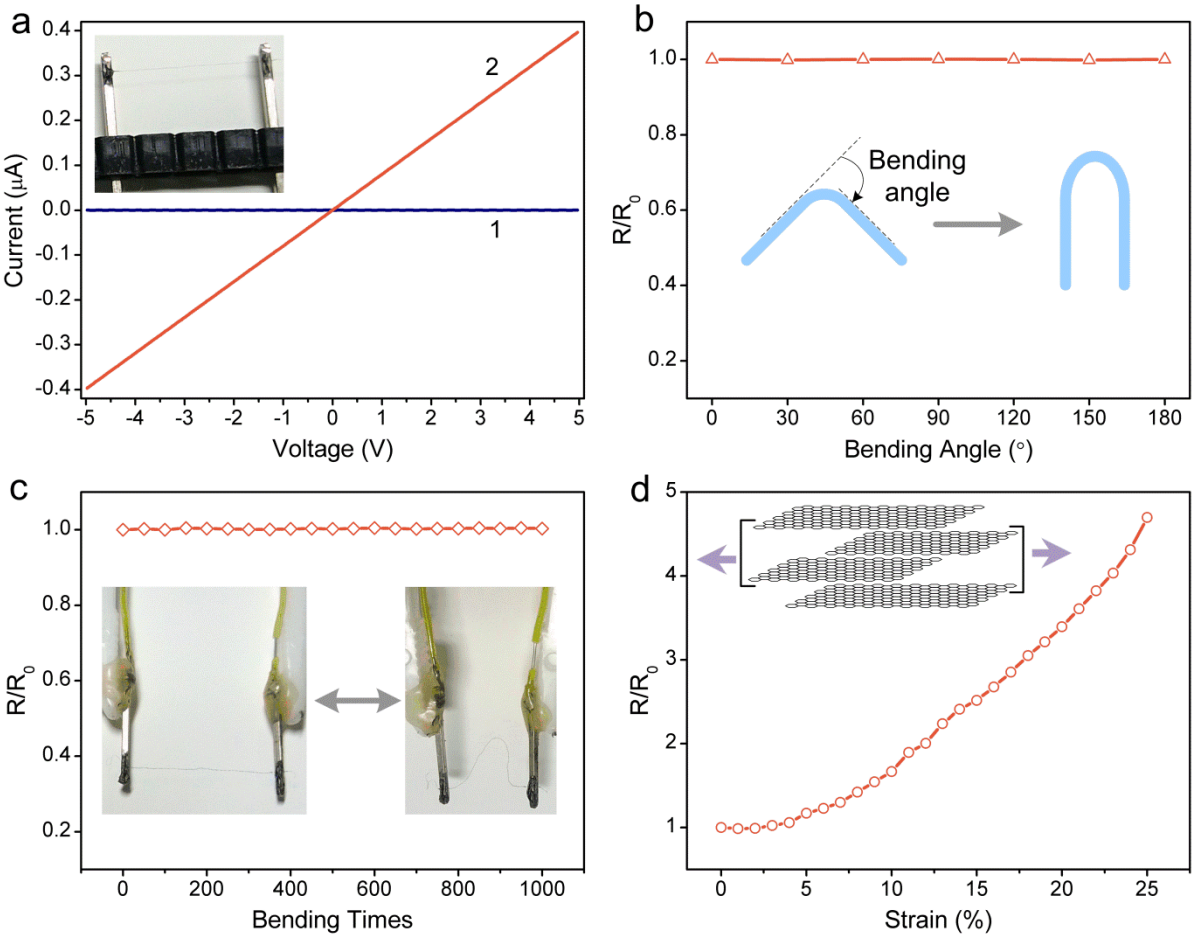

Fig. 3 (a) I-V curves of a pure silk fibre (1) and a graphene coated silk fibre (2), inset shows a digital photograph of a graphene coated silk fibre fixed across two electrodes. (b) The normalized resistance change according to the bending angle of the fibre. (c) The normalized resistance change according to the bending times; insets are photos of a graphene coated silk fibre before and after bending. (d) Normalized resistance of a graphene coated silk fibre under stretching; inset illustrates the overlap of graphene sheets.

Electrical property of graphene coated silk fibre

To investigate the electrical property of graphene coated silk fibre. A single graphene coated silk fibre was placed across two copper electrodes (Fig. 3a inset and Fig. S5). The separation between the two electrodes was 10 mm. The ends of the fibre were bonded to the electrodes with conductive carbon paint. The fibre was stretched slightly to make it straight. Fig. 3a shows the I-V curves of a silk fibre and a graphene coated silk fibre. It is clear that graphene coating of the fibre results in considerable changes to the I-V characteristics and that there is an enhanced electronic conduction in the fibre, indicating graphene sheets are successfully coated on the silk fibre. It is observed that within the voltage range measured, the electronic conduction of the graphene coated silk fibre shows Ohm behaviour without nonlinearity. The resistance of the fibre was measured from the slope of the I-V curve to be 12.5 MΩ cm^{-1}. This high resistance might be resulted from electron tunnelling and hopping between graphene sheets. Increasing the graphene coating layer can decrease the resistance. For example, the silk fibre coated with graphene twice has a resistance about 2.2 MΩ cm^{-1} (57.9 S m^{-1}) in our study, which is lower than that of a 10 nm thin gold layer coated silk fibre.[36] Thick gold layer coating can leads to much lower resistance, but it will cause a loss in fibre elasticity.

The resulted graphene coated silk fibres are very flexible, elastic and tough. To investigate the electrical resistance of graphene coated silk fibres under bending condition, two ends of a fibre were paste on two electrodes which were fixed on an insulating tweezers respectively (Fig. 3c inset). Bending was

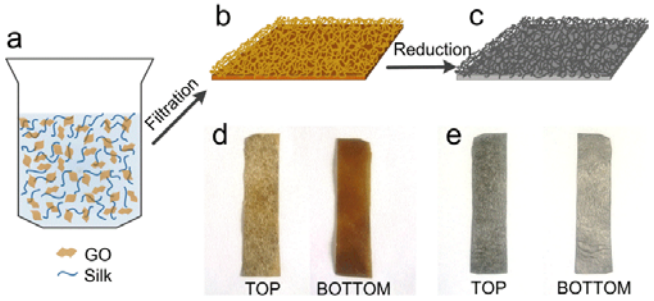

Fig. 4 Schematic illustration of the fabrication of G/S films. (a) GO and silk fibre suspension. (b) GO/S film obtained after vacuum filtration. (c) G/S film obtained after reduction. (d) A digital photograph of the top and bottom side of a GO/S film. (e) A digital photograph of the top and bottom side of a G/S film.

operated by hand. As shown in Fig. 3b, the normalized resistance (R/R0) variations are very little under different bending angles. What's more, during 1000 times bending, the conductivities of graphene coated silk fibre were stable and showed a negligible fluctuation (Fig. 3c). The electrical conductance of the graphene coated silk fibre under strain was also investigated. For stretch test, the two electrodes were fixed on the jaws of a digital calliper. Stretch was made by sliding a jaw, and the length change of the fibre was directly read from the digital display. As shown in Fig. 3d, the normalized resistance change was unnoticeable below 5% elongation. Stretching from 5% to 25% increased the normalized resistance almost linearly. The resistance increasing might be due to that graphene sheets covering on the silk surface were overlapped as illustrated in Fig. 3d inset. During the stretch, the area of the overlap was decreased, and the resistance was increased. When the strain exceeded 25%, the fibre was broken.

Morphology of G/S composite films

As illustrated in Fig. 4a-c, a graphene oxide/silk composite (GO/S) film was firstly fabricated by filtration of a GO and silk

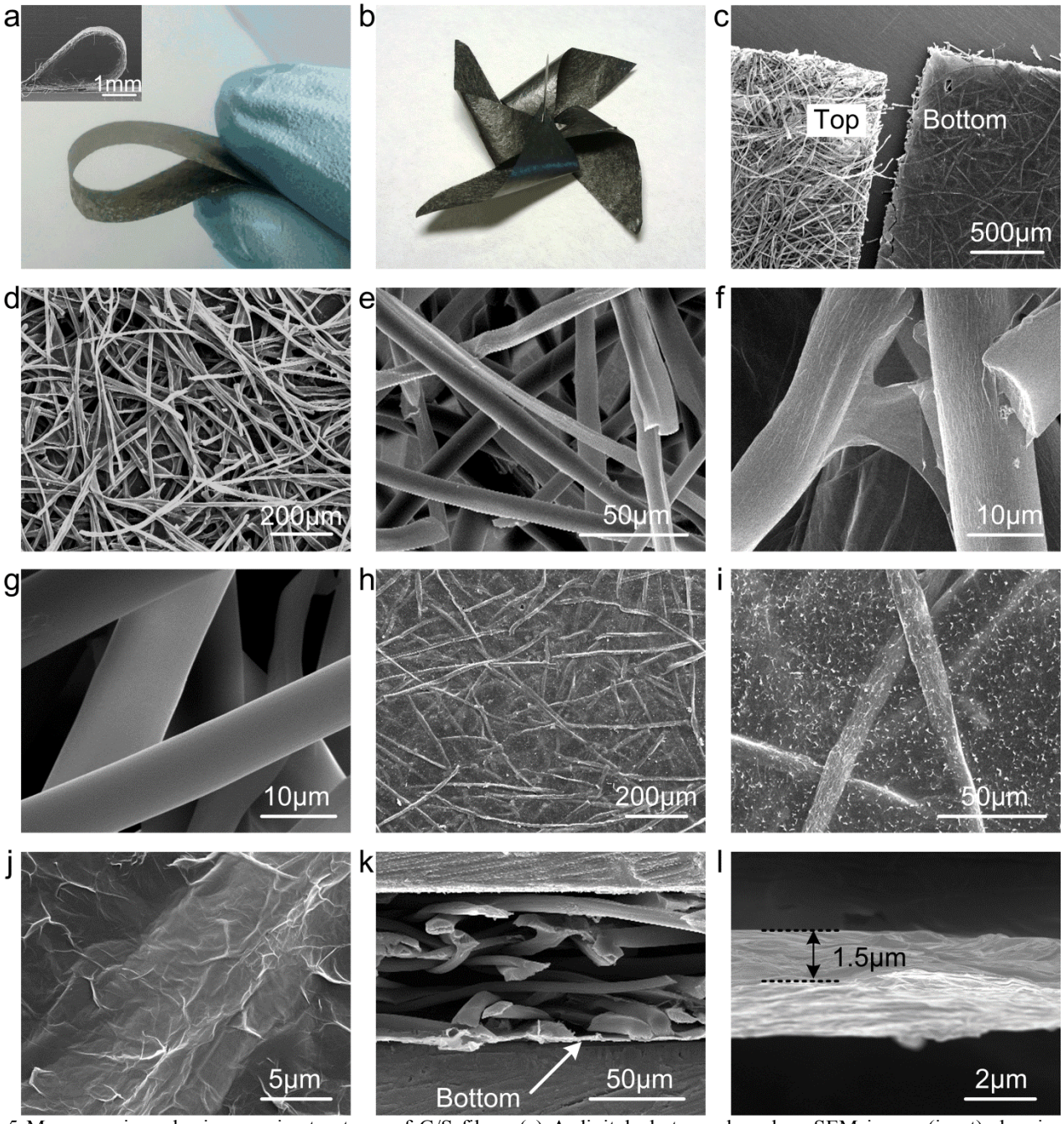

Fig. 5 Macroscopic and microscopic structures of G/S films. (a) A digital photograph and an SEM image (inset) showing the flexibility of the G/S film. (b) A pinwheel made of a 9 cm^2 G/S film. (c) A low-magnification SEM image of two pieces G/S films with top and bottom side up respectively. (d-f) SEM images of the top side of a G/S film with different magnifications. (g) An SEM image of pure silk fibres. (h-j) SEM images of the bottom side of a G/S film with different magnifications. (k) A side-view SEM image of a G/S film. (l) A high-magnification SEM image of the bottom layer of a G/S film.

fibre suspension through a membrane filter, followed by air drying and peeling off from the filter. The GO/S film has two different sides, top side rough and sand yellow, while bottom side smooth and dark brown, as shown in Fig. 4d. The GO/S film was further reduced in ascorbic acid solution in a boiling water bath for 2 h and dried at 65 ℃ in air for 2 h. The colour of the composite film turned to black and a double-faced G/S film was obtained. As shown in Fig. 4e, top side of the G/S film is rough and black, while the bottom side is smooth and displays a shiny metallic lustre, which is different from previously reported graphene films that display a shiny metallic lustre on both sides.[22]

The prepared G/S film is free-standing and highly flexible (Fig. 5a, b).The morphology differences between top side and bottom side of the G/S film were confirmed by SEM images with different magnifications (Fig. 5c-j). As shown, the top side of the G/S film shows hierarchical network structured silk fibres (Fig. 5d,e) while the bottom side of the G/S film shows a smooth surface with a silk fibre network buried under the graphene sheets (Fig. 5h-j). The diameter of silk fibres is 10 to 15 μm, while the average length of the fibres is 2 mm. The high magnification SEM images show that silk fibres are coated with graphene and have a wrinkled surface (Fig. 5f) in contrast to pure silk fibres that are very smooth (Fig. 5g). Graphene coating make the silk fibres electrical conductive and the sheet resistivity measured from the top side of the G/S film is 650 Ω □$^{-1}$. The high magnification SEM image of the bottom side of G/S film shows a wrinkled surface (Fig. 5j) with silk fibres buried in the graphene layers. The sheet resistivity measured from the bottom side is 90 Ω □$^{-1}$, which is dramatically lower than that from the top side. This good electrical conducting property makes the bottom layer of G/S film act like a current collector in supercapacitor and electrochemical sensor applications. The fracture edge of the G/S film exhibits a hierarchical structure with a loose top layer and a compact bottom layer (Fig. 5k). The total thickness of the G/S film is about 70 μm which is mainly contributed by the top layer. The thickness of the bottom layer is about 1.5 μm (Fig. 5l). Various G/S films with different thickness were obtained with different amount of silk fibres (Fig. S6). The formation of the heterogeneous film might be due to the large pore size (>10 μm) of the silk fibre network. GO sheets could penetrate the fibre network and precipitated on the filter membrane to form the bottom layer of the GO/S film. The mechanical flexibility of the G/S film was quantitatively examined using tensile test. The stress-strain curve shows the G/S film can withstand a stress of 3.5 MPa with a 1.2 % elongation (Fig. S7). The combination of porous top layer and compact bottom layer in a single G/S film let it can be directly used as electrochemical electrodes without needs of any additional binders or conductive additives and leads to a simplified and lightweight architecture.

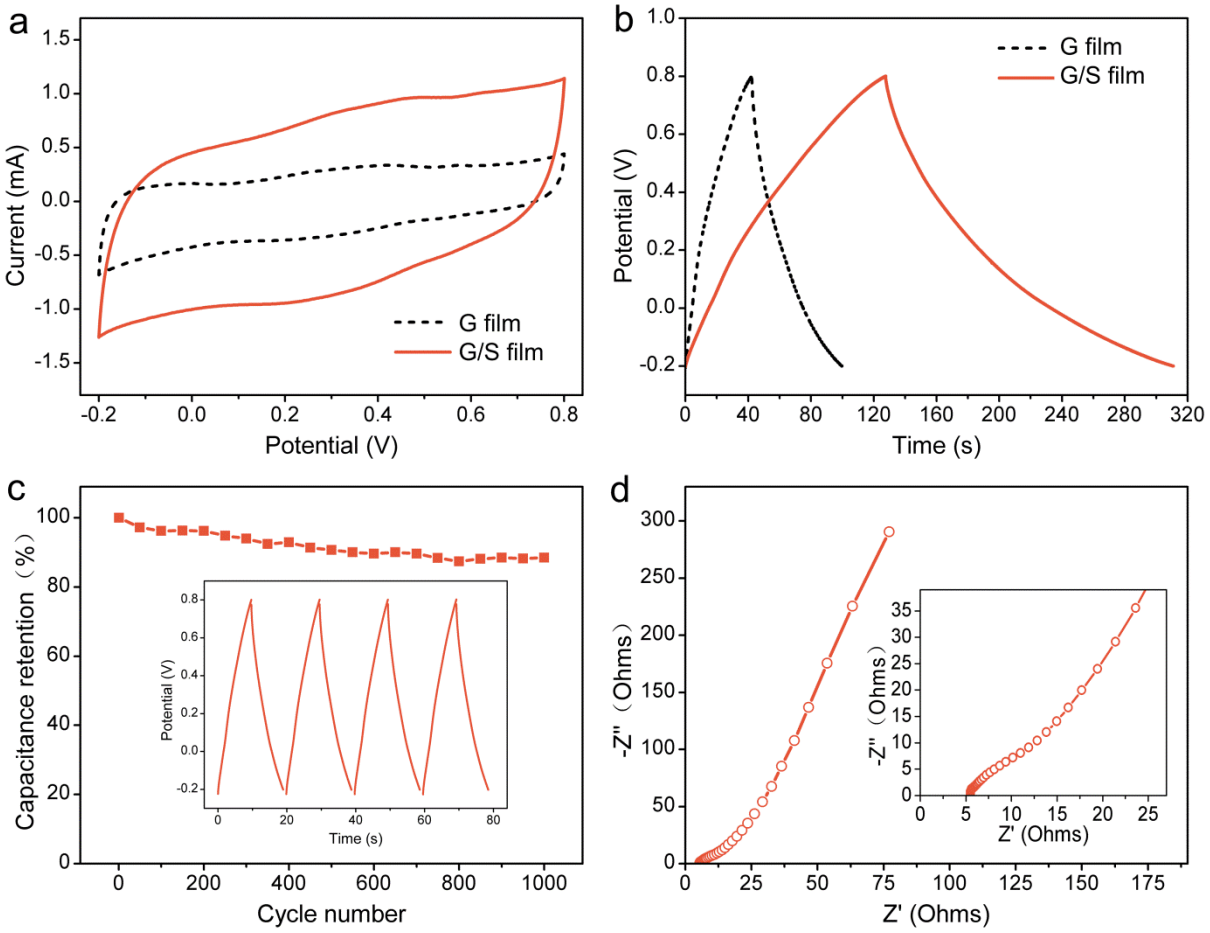

Fig. 6 (a) CV curves of the G and G/S film at a scan rate of 100 mV s^{-1}. (b) Galvanostatic charge/discharge curves of the G and G/S film at a current density of 1 A g^{-1}. (c) Cycle stability of the G/S film during the long-term charge/discharge process at a current density of 10 A g^{-1}. Inset shows the Galvanostatic charge/discharge curves of the G/S film at a current density of 10 A g^{-1}. (d) Nyquist plots of the impedance of a G/S film. Inset showing the corresponding magnified high-frequency regions.

Electrochemical performance of the G/S film

The produced G/S films are mechanically robust, show high conductivity and can thus be directly used as electrochemical electrodes. The electrochemical performance of a G/S film was analysed through cyclic voltammetry (CV), electrochemical impedance spectroscopy, and galvanostatic charge/discharge experiments with the G/S film as a work electrode, an Ag/AgCl as a reference electrode and a Pt electrode as a counter electrode. 1M H_2SO_4 was use as the aqueous electrolyte. Cyclic voltammetry and galvanostatic charge-discharge were performed over the potential range of -0.2 V to 0.8 V with scan rates 100 mV s^{-1} to 500 mV s^{-1} and currents densities 1 A g^{-1} and 10 A g^{-1} with respect to graphene, respectively. As shown in Fig. 6a, in comparison with a pure graphene film (G film), the G/S film shows an enhanced electrochemical performance with a nearly rectangular CV shape at a scan rate of 100 mV s^{-1}. Additionally, the G/S film is robust enough to be charged and discharged over a wide range of scan rates (100 to 500 mV s^{-1}) and still maintains its nearly rectangular CV shape (Fig. S8).

Fig. 6b shows the galvanostatic charge/discharge curves obtained at a current density of 1 A g^{-1} of G and G/S film. The areal capacitance of the G/S film was calculated to be 17.75 mF cm^{-2} which is two-fold higher than that of the G film (5.72 mF cm^{-2}), indicating the large activity specific surface area of the G/S film. Additionally, the G/S film electrode retained 89% of its initial capacitance after 1000 cycles at a high current density of 10 A g^{-1} (Fig. 6c). Electrochemical impedance spectroscopy of the G/S film shows a low electron transfer resistance (Rct) (Fig. 6d), indicating fast ion transport within the G/S film electrode.

The enhanced electrochemical performance of the G/S film should be attributed to its special structure. First, the graphene coated silk fibres in the top layer of the G/S film provide the large and accessible specific surface area for charge storage. Then, the network structured top layer of the G/S film has open pores, which helps facilitate the electrolyte accessibility to the electrode surfaces. Last, the bottom layer of the G/S film retains excellent electronic conductivity and directly acts as a current collector, which ensures the high-performance of the electrochemical electrode.

The electrochemical performances of G/S films prepared with different ratio of GO to silk were also studied. Fig.S9 shows the area of CV curves of G/S films raised according to the silk fibre amount. The reason might be that more silk fibres leading to more loose structure and more electrode surface area. However, too much silk fibres could reduce the mechanical properties of the composite film. Moreover, the electrochemical performances of G/S film could be enhanced by preparing the film with more GO amount (Fig. S10). That's because more graphene sheets in the film provided much more accessible surface area for charge storage.

Pt nanosphere deposition and H_2O_2 detection

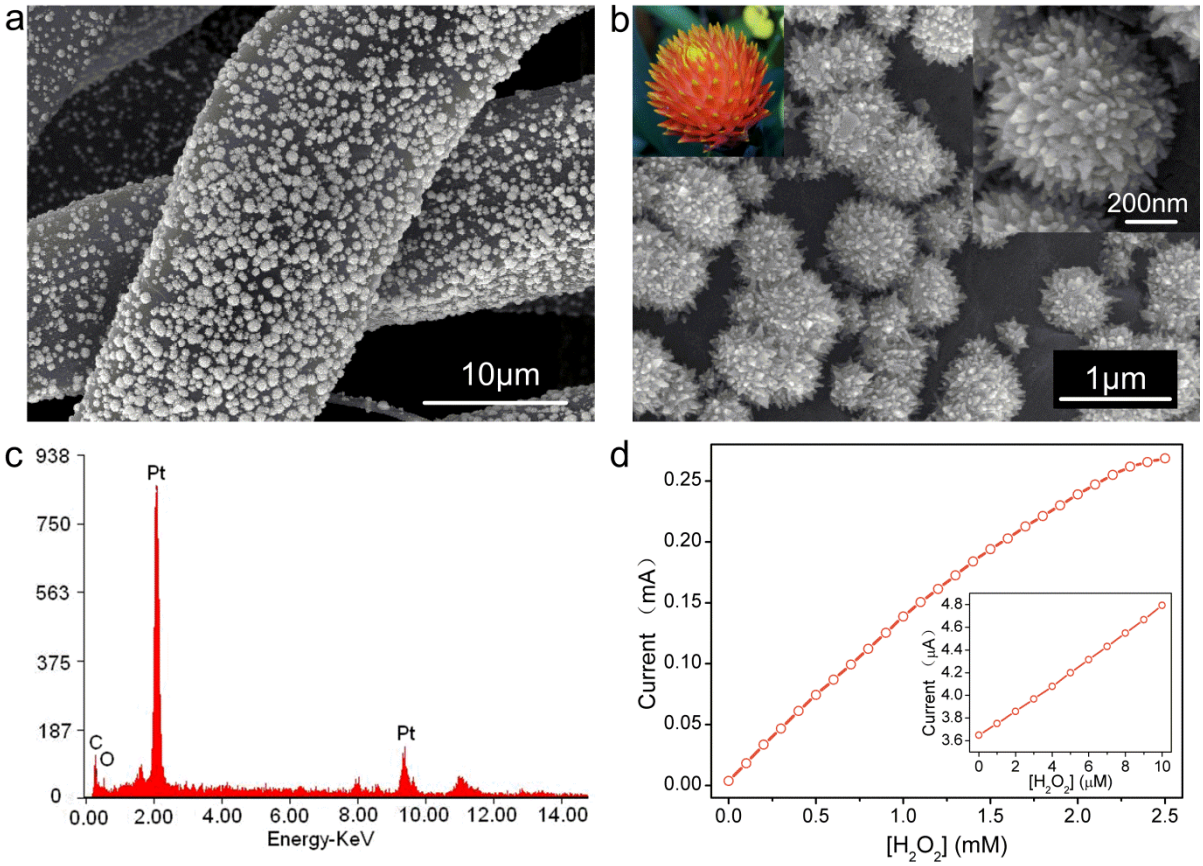

Fig. 7 (a) An SEM image of a G/S film decorated with Pt nanosphere. (b) A high-magnification SEM image of the G/S film decorated with Pt nanosphere. Inset right shows a Pt spiky nanosphere and inset left shows a photograph of a spiky flower heed that is similar to the Pt nanosphere. (c) EDX spectrum of the Pt nanosphere decorated G/S film. (d) Calibration curve of H_2O_2 detection of the Pt nanosphere decorated G/S film at 0.65 V vs. Ag/AgCl. Inset shows the enlarged calibration curve at low H_2O_2 concentration (1 μM to 10 μM).

In order to demonstrate the electrochemical sensor application of G/S films, we fabricated a H_2O_2 sensor by depositing Pt nanospheres on a G/S film. H_2O_2 is an important by-product of many analyte-specific enzymes, as well as a known brain neuromodulator.[47, 48] The deposition of Pt nanospheres was performed by CV scanning in the potential range from 0 to -0.6 V. Fig. 7a displays an SEM image of Pt nanospheres grown on the surface of graphene coated silk fibres. The high magnification SEM images reveal that Pt nanospheres have a spiky ball structure (Fig. 7b and Fig. S11) that is similar to a spiky flower heed (Fig. 7b, inset left). The typical diameter of the nanosphere is about 700 nm with sharp spikes about 50 nm (Fig. 7b, inset right). EDX spectrum confirms the presence of Pt on the G/S film (Fig. 7c). However, no spiky nanostructure has been observed when Pt nanoparticles deposited on pure G film and the bottom side of the G/S film (Fig. S12). The reason might be that the thin graphene sheets covered on the silk fibre surface provide scattered nucleation sites for Pt electrodeposition and facilitate nuclei growing. While the compact graphene film has densely distributed nucleation sites resulting in overlapping of the diffusion fields of the individual Pt nuclei. This interparticle diffusion coupling effect inhibits the nuclei growing.[49, 50]

The Pt nanosphere decorated G/S film was directly used as a H_2O_2 detection electrode. Amperometric experiments for H_2O_2 detection were performed in a stirred PBS solution (pH 7.4, 0.01 M) in a three-electrode system with an Ag/AgCl reference electrode and a Pt counter electrode. After an initial background stabilization period of 900 s, the concentration of H_2O_2 was sequentially raised from 0 to 2.5 mM every 60 s by dropping 25 µL 0.1 M H_2O_2 aqueous solution to 25 mL PBS. Fig. 7d shows the amperometric response as a function of H_2O_2 concentration at 0.65 V vs. Ag/AgCl. The sensor response is linear to H_2O_2 concentrations in the range from 0.1 mM to 2.0 mM with a detection sensitivity of 0.56 mA mM^{-1} cm^{-2} which is twice as high as that of Pt deposited G film (Fig. S13). The inset of Fig. 7e shows the calibration curve of H_2O_2 detection at low H_2O_2 concentrations from 1 µM to 10 µM with a detection limit as low as 0.2 µM (S/N=3) .

Glucose detection performance

Glucose biosensors have attracted a great deal of attention due to the practical medical needs for diabetes diagnosis.[51-53] Here, we prepared a glucose biosensor by immobilizing glucose oxidases (GOx) on a Pt nanosphere decorated G/S film (Fig.S14). Amperometric experiments for glucose detection were similar to that of H_2O_2 detection. After an initial

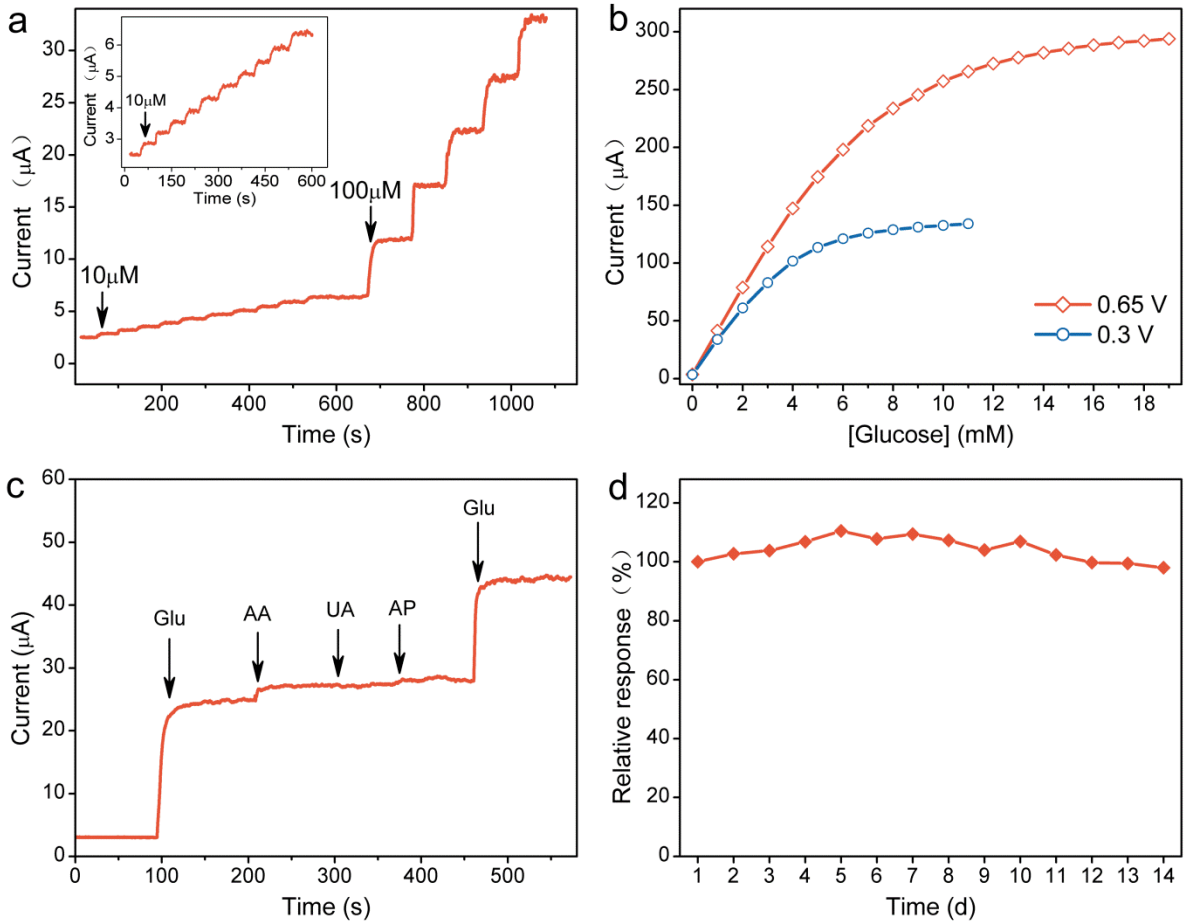

Fig. 8 (a) Amperometric response of the GOx immobilized G/S film to successive addition of 10 µM and 100 µM glucose concentration. Inset shows the amperometric response at low glucose concentration (10 µM to 100 µM). (b) Calibration curve of glucose detection at the applied potential of 0.65 V and 0.3 V vs. Ag/AgCl. (c) Amperometric response curve of GOx immobilized G/S film to additions (indicated with arrows) of 1mM of glucose (Glu), 0.1mM of ascorbic acid (AA) 0.1mM of uric acid (UA), 0.1mM of acetaminophen (AP), and 1mM of glucose (Glu) at 0.3 V vs. Ag/AgCl. (d) Variation of the current response of GOx immobilized G/S film to 4 mM glucose with time.

background stabilization period of 900 s, the concentration of glucose was sequentially raised from 0 to 19 mM every 60 s by dropping 25 μL 1 M glucose aqueous solution to 25 mL PBS. For low concentration detection, concentration increments of 10 μM and 100 μM were realized by dropping 0.25 μL and 2.5 μL 1 M glucose to 25 mL PBS by a microliter syringe respectively. Fig. 8a shows the typical amperometric response of the glucose biosensor upon the successive injection of glucose at an applied potential of 0.65 V vs. Ag/AgCl. The sensitivity of the glucose sensor is as high as 150.8 μA mM^{-1} cm^{-2} which makes the glucose sensor quite adequate to detect ultra-low glucose concentration (Fig. 8a, inset) and the detection limit of the sensor is estimated to 1 μM (S/N=3). The linear response range is about 10 μM to 10 mM (Fig. 8b). The comparison of the analytical performance of the developed electrode with other graphene based glucose sensors reported previously was summarized in Table S1. It can be seen that the G/S film based glucose biosensor exhibits a higher sensitivity and a lower detection limit. When the applied potential decreased to 0.3 V vs. Ag/AgCl, the glucose biosensor still has a fine amperometric response to glucose as shown in Fig. 8b. Moreover, at this low potential, the sensor shows negligible response to 0.1mM additions of ascorbic acid (AA), uric acid (UA) and acetaminophen (AP) respectively while the current responses of glucose are quickly and obviously (Fig. 8c), indicating that the resultant glucose biosensor is highly selective for glucose detection. The stability of the biosensor has also been investigated by periodically recording its current response to 4 mM glucose. The response current of the electrode retained 98% of its initial response after two weeks (Fig. 8d). What's more, the electrodes showed a little variation of current response under bending condition (Fig. S15 a) and maintain 94% of its initial current response to 4 mM glucose after bent for 200 times (Fig. S15 b).

Such high performance of the H_2O_2 and glucose detection benefited from the hierarchical network structure of the G/S film. Graphene coated silk fibres on the G/S film provide a large and accessible surface area for Pt nanosphere decoration and GOx immobilization. The porous structure of the top layer also makes the diffusion of analytes to the electrode surface more easily and rapidly.

Conclusions

In summary, we have coated graphene sheets on silk fibres to make them electrical conductive and investigated the electrical and mechanical properties of a single graphene coated silk fibre. A double-faced G/S film has been fabricated, possessing a porous and hierarchical top layer and a compact, mechanically strong, flexible and electrically conductive bottom layer. The free-standing G/S film can be directly used as an electrochemical electrode with high performance. As spiky Pt nanospheres grown on the G/S film, the electrode showed high sensitivity and low detection limit for H_2O_2 detection. A glucose biosensor has been prepared by immobilizing GOx enzyme on the Pt nanosphere decorated G/S film with good detection performance at ultra-low glucose concentrations. What's more, the combination of hierarchical porous network structure, mechanical flexibility, and electrically conductivity makes the G/S film very promising for many applications, such as cell sensors, tissue engineering scaffolds, microbial fuel cells, bendable electrodes, and wearable biomedical devices.

Acknowledgements

This work was financially supported by the National Key Technology R&D Program of China (No. 2012BAI16B02), the National Natural Science Foundation of China (Nos. 81171416, 60875078)

Notes and references

Biosensor National Special Laboratory, College of Biomedical Engineering and Instrument Science, Cyrus Tang Centre for Sensor Materials and Applications, Zhejiang University，Hangzhou 310027, PR China. E-mail: yexuesong@zju.edu.cn

† Electronic Supplementary Information (ESI) available. See DOI: 10.1039/b000000x/

1. C. Keplinger, J.-Y. Sun, C. C. Foo, P. Rothemund, G. M. Whitesides and Z. Suo, *Science*, 2013, **341**, 984-987.
2. M. Kaltenbrunner, T. Sekitani, J. Reeder, T. Yokota, K. Kuribara, T. Tokuhara, M. Drack, R. Schwödiauer, I. Graz and S. Bauer-Gogonea, *Nature*, 2013, **499**, 458-463.
3. W.-Y. Wu, X. Zhong, W. Wang, Q. Miao and J.-J. Zhu, *Electrochem. Commun.*, 2010, **12**, 1600-1604.
4. F. Xiao, Y. Li, H. Gao, S. Ge and H. Duan, *Biosens. Bioelectron.*, 2012, **41**, 417-423.
5. G. S. Jeong, D.-H. Baek, H. C. Jung, J. H. Song, J. H. Moon, S. W. Hong, I. Y. Kim and S.-H. Lee, *Nat. Commun.*, 2012, **3**, 977.
6. R. Verplancke, F. Bossuyt, D. Cuypers and J. Vanfleteren, *J. Micromech. Microeng.*, 2012, **22**, 015002.
7. D.-H. Baek, J. S. Park, E.-J. Lee, S. J. Shin, J.-H. Moon, J. J. Pak and S.-H. Lee, *IEEE Trans. Biomed. Eng.*, 2011, **58**, 1466-1473.
8. X. Huang, Z. Zeng, Z. Fan, J. Liu and H. Zhang, *Adv. Mater.*, 2012, **24**, 5979-6004.
9. X. Huang, X. Qi, F. Boey and H. Zhang, *Chem. Soc. Rev.*, 2012, **41**, 666-686.
10. Q. He, S. Wu, Z. Yin and H. Zhang, *Chemical Science*, 2012, **3**, 1764-1772.
11. X. Huang, S. Li, Y. Huang, S. Wu, X. Zhou, S. Li, C. L. Gan, F. Boey, C. A. Mirkin and H. Zhang, *Nat. Commun.*, 2011, **2**, 292.
12. X. Huang, S. Li, S. Wu, Y. Huang, F. Boey, C. L. Gan and H. Zhang, *Adv. Mater.*, 2012, **24**, 979-983.
13. F. Xiao, J. Song, H. Gao, X. Zan, R. Xu and H. Duan, *Acs Nano*, 2011, **6**, 100-110.
14. F. Liu, S. Song, D. Xue and H. Zhang, *Adv. Mater.*, 2012, **24**, 1089-1094.
15. H. Gwon, H.-S. Kim, K. U. Lee, D.-H. Seo, Y. C. Park, Y.-S. Lee, B. T. Ahn and K. Kang, *Energ. Environ. Sci.*, 2011, **4**, 1277-1283.
16. C. Wang, D. Li, C. O. Too and G. G. Wallace, *Chem. Mater.*, 2009, **21**, 2604-2606.
17. D.-W. Wang, F. Li, J. Zhao, W. Ren, Z.-G. Chen, J. Tan, Z.-S. Wu, I. Gentle, G. Q. Lu and H.-M. Cheng, *Acs Nano*, 2009, **3**, 1745-1752.
18. Y.-R. Kang, Y.-L. Li, F. Hou, Y.-Y. Wen and D. Su, *Nanoscale*, 2012, **4**, 3248-3253.
19. X. Huang, Z. Yin, S. Wu, X. Qi, Q. He, Q. Zhang, Q. Yan, F. Boey and H. Zhang, *Small*, 2011, **7**, 1876-1902.
20. G. Wang, X. Sun, F. Lu, H. Sun, M. Yu, W. Jiang, C. Liu and J. Lian, *Small*, 2012, **8**, 452-459.

21. X. Yang, J. Zhu, L. Qiu and D. Li, *Adv. Mater.*, 2011, **23**, 2833-2838.
22. H. Chen, M. B. Müller, K. J. Gilmore, G. G. Wallace and D. Li, *Adv. Mater.*, 2008, **20**, 3557-3561.
23. A. C. Neto, F. Guinea, N. Peres, K. S. Novoselov and A. K. Geim, *Rev. Mod. Phys.*, 2009, **81**, 109.
24. D. Li, M. B. Mueller, S. Gilje, R. B. Kaner and G. G. Wallace, *Nat. Nanotechnol.*, 2008, **3**, 101-105.
25. A. K. Geim, *Science*, 2009, **324**, 1530-1534.
26. X.-F. Teng, Y.-T. Zhang, C. C. Poon and P. Bonato, *IEEE Rev. Biomed. Eng.*, 2008, **1**, 62-74.
27. C. Goy, J. Dominguez, M. Gómez López, R. Madrid and M. Herrera, *J. Med. Eng. Technol.*, 2013, **37**, 359-367.
28. S. Jiang, E. Newton, C. Yuen and C. Kan, *Text. Res. J.*, 2006, **76**, 57-65.
29. H. M. Lee, S. Y. Choi, A. Jung and S. H. Ko, *Angew. Chem. Int. Ed.*, 2013, **52**, 7718-7723.
30. N. L. Silva, L. Gonçalves and H. Carvalho, *J. Mater. Sci: Mater. Electron.*, 2013, **24**, 635-643.
31. J. Molina, J. Fernández, A. del Río, J. Bonastre and F. Cases, *Appl. Surf. Sci.*, 2013, **279**, 46-54.
32. L. Hu, M. Pasta, F. L. Mantia, L. Cui, S. Jeong, H. D. Deshazer, J. W. Choi, S. M. Han and Y. Cui, *Nano lett.*, 2010, **10**, 708-714.
33. G. H. Altman, F. Diaz, C. Jakuba, T. Calabro, R. L. Horan, J. Chen, H. Lu, J. Richmond and D. L. Kaplan, *Biomaterials.*, 2003, **24**, 401-416.
34. Y. Xia, X. Lu and H. Zhu, *Compos. Sci. Technol.*, 2013, **77**, 37-41.
35. E. Steven, J. G. Park, A. Paravastu, E. B. Lopes, J. S. Brooks, O. Englander, T. Siegrist, P. Kaner and R. G. Alamo, *Sci. Technol. Adv. Mat.*, 2011, **12**, 055002.
36. P. Morales, B. Rapone, M. Caruso and D. Flammini, *Nanotechnology*, 2012, **23**, 255304.
37. L. Huang, C. Li, W. Yuan and G. Shi, *Nanoscale*, 2013, **5**, 3780-3786.
38. K. Hu, M. K. Gupta, D. D. Kulkarni and V. V. Tsukruk, *Adv. Mater.*, 2013, **25**, 2301-2307.
39. L. Malard, M. Pimenta, G. Dresselhaus and M. Dresselhaus, *Phys. Rep.*, 2009, **473**, 51-87.
40. K. N. Kudin, B. Ozbas, H. C. Schniepp, R. K. Prud'Homme, I. A. Aksay and R. Car, *Nano lett.*, 2008, **8**, 36-41.
41. L. Qiu, J. Z. Liu, S. L. Chang, Y. Wu and D. Li, *Nat. Commun.*, 2012, **3**, 1241.
42. H. Feng, R. Cheng, X. Zhao, X. Duan and J. Li, *Nat. Commun.*, 2013, **4**, 1539.
43. S. Park, J. An, I. Jung, R. D. Piner, S. J. An, X. Li, A. Velamakanni and R. S. Ruoff, *Nano lett.*, 2009, **9**, 1593-1597.
44. S. Stankovich, D. A. Dikin, R. D. Piner, K. A. Kohlhaas, A. Kleinhammes, Y. Jia, Y. Wu, S. T. Nguyen and R. S. Ruoff, *Carbon*, 2007, **45**, 1558-1565.
45. P. Monti, P. Taddei, G. Freddi, T. Asakura and M. Tsukada, *J. Raman. Spectrosc.*, 2001, **32**, 103-107.
46. P. Monti, G. Freddi, A. Bertoluzza, N. Kasai and M. Tsukada, *J. Raman. Spectrosc.*, 1998, **29**, 297-304.
47. S. Vaddiraju, I. Tomazos, D. J. Burgess, F. C. Jain and F. Papadimitrakopoulos, *Biosens. Bioelectron.*, 2010, **25**, 1553-1565.
48. L. Qiang, S. Vaddiraju, D. Patel and F. Papadimitrakopoulos, *Biosens. Bioelectron.*, 2011, **26**, 3755-3760.
49. R. M. Penner, *J. Phys. Chem. B*, 2002, **106**, 3339-3353.
50. A. Kloke, F. von Stetten, R. Zengerle and S. Kerzenmacher, *Adv. Mater.*, 2011, **23**, 4976-5008.
51. N. Oliver, C. Toumazou, A. Cass and D. Johnston, *Diabetic. Med.*, 2009, **26**, 197-210.
52. J. Wang, *Chem. Rev.*, 2008, **108**, 814-825.
53. B. Liang, L. Fang, G. Yang, Y. Hu, X. Guo and X. Ye, *Biosens. Bioelectron.*, 2013, **43**, 131-136.

